Δ98Δ, a Functional All-β-Sheet Abridged Form of Intestinal Fatty Acid Binding Protein†

Lucrecia M. Curto, Julio J. Caramelo,‡ and José M. Delfino*

Department of Biological Chemistry and Institute of Biochemistry and Biophysics (IQUIFIB), School of Pharmacy and Biochemistry, University of Buenos Aires, Junín 956, C1113AAD, Buenos Aires, Argentina

Received June 6, 2005; Revised Manuscript Received August 25, 2005

ABSTRACT: Intestinal fatty acid binding protein (IFABP) is a 15 kDa intracellular lipid-binding protein exhibiting a β-barrel fold that resembles a clamshell. The β-barrel, which encloses the ligand binding cavity, consists of two perpendicular five-stranded β-sheets with an intervening helix-turn-helix motif between strands A and B. Δ98Δ (fragment 29−126 of IFABP) was obtained either in its recombinant form or by limited proteolysis with clostripain. Despite lacking extensive stretches involved in the closure of the β-barrel, Δ98Δ remains soluble and stable in solution. Spectroscopic analyses by circular dichroism, ultraviolet absorption, and intrinsic fluorescence indicate that the fragment retains substantial β-sheet content and tertiary interactions. In particular, the environment around W82 is identical in both Δ98Δ and IFABP, a fact consistent with the conservation in the former of all the critical amino acid residues belonging to the hydrophobic core. In addition, the Stokes radius of Δ98Δ is similar to that of IFABP and 16% larger than that calculated from its molecular weight (11 kDa). The monomeric status of Δ98Δ was further confirmed by chemical cross-linking experiments. Although lacking 25% of the amino acids of the parent protein, in the presence of GdnHCl, Δ98Δ unfolds through a cooperative transition showing a midpoint at 0.90 M. Remarkably, it also preserves binding activity for fatty acids (K_d = 5.1 μM for oleic acid and K_d = 0.72 μM for trans-parinaric acid), a fact that exerts a stabilizing effect on its structure. These cumulative evidences show that Δ98Δ adopts a monomeric state with a compact core and a loose periphery, being so far the smallest structure of its kind preserving binding function.

Fatty acid binding proteins (FABPs) belong to the intracellular lipid-binding proteins (iLBPs) family. FABPs share a similar β-barrel fold that resembles a clamshell. This β-barrel, which encloses the ligand binding cavity, consists of two five-stranded β-sheets arranged in a nearly orthogonal orientation. This structure differs from most globular proteins since its interior is occupied by a large solvent-filled cavity, while the hydrophobic core is small and displaced from the protein center. All β-strands are connected by loops with the exception of strands A and B (see Figure 3), where an intervening helix-turn-helix motif appears (*1*). Given their unusual features, FABPs are a useful model to study the structure and dynamics of β-sheet proteins. In particular, intestinal fatty acid binding protein (IFABP)[1] is a monomeric protein of 131 amino acids (15 kDa) devoid of C or P residues, thereby avoiding two major problems that complicate the analysis of protein folding (*2*).

In accordance with the picture provided by NMR, the structure of apo-IFABP (the protein without ligand)—and in contrast to holo-IFABP—shows local disorder at the distal half of α-helix II, the αII−βB linker, and the βC−βD turn. These regions, plus the βE−βF turn, undergo fluctuations postulated to be necessary for binding and release of ligands, in a mechanism known as the "dynamic portal hypothesis" (*3*). Two variants of helix-less IFABP (Δ17-SG and Δ27-GG) show that the helical domain is not necessary to preserve the general topology of IFABP (*4*, *5*). Interestingly, these proteins retain the ability to bind fatty acids, although with a lesser affinity than the full-length protein, indicating that the helical domain contributes to regulate the affinity of the protein for different fatty acids. On the other hand, deletion of the last three C-terminal residues of IFABP results in a monomeric and compact nonnative state (*6*). In this sense, to define the minimal sequence compatible with a stable fold and binding activity is an issue with general implications for protein folding and function in this class of proteins.

Previous work (*3*, *7*, *8*) showed that IFABP is in equilibrium between at least two major conformations with different flexibility at the helical domain, namely, a flexible open state and a closed more rigid state. These forms present differential susceptibility to proteolysis, holo-IFABP (the form bound to oleic acid) being the most resistant species, a fact consistent with a more ordered conformation. Remarkably,

† This research has been supported by grants from the University of Buenos Aires (UBA), the Consejo Nacional de Investigaciones Científicas y Técnicas (CONICET), the Agencia Nacional de Promoción Científica y Tecnológica (ANPCyT), and from the Comisión Nacional de Programas de Investigación Sanitaria (CONAPRIS).

* To whom correspondence should be addressed. E-mail: delfino@qb.ffyb.uba.ar. Tel: 54 11 4964-8289. Fax: 54 11 4962-5457.

‡ Current address: Laboratory of Glycobiology, Fundación Instituto Leloir, Av. Patricias Argentinas 435, C1405BWE, Buenos Aires, Argentina.

[1] Abbreviations: Δ98Δ, a truncated variant of IFABP corresponding to the fragment 29−126 of the parent protein; IFABP, intestinal fatty acid binding protein; apo- or holo-, prefixes that denote the absence or presence of fatty acid ligand.

10.1021/bi051080s CCC: $30.25
Published on Web 09/29/2005

the main fragment generated from proteolysis with clostripain of holo-IFABP is highly resistant to further degradation. It was then postulated that stability to proteolysis of this 11 kDa fragment is due to its ability to bind the ligand, a feature that would help it remain structured. Here, we present the making and structural characterization of Δ98Δ, the shortest form of IFABP described so far preserving binding activity.

EXPERIMENTAL PROCEDURES

Materials. Rat IFABP cDNA, coded in the plasmid pET-11a, was expressed in *Escherichia coli* strain BL21(DE3), and the protein was purified as described previously (*8*). Recombinant Δ98Δ was cloned by PCR using primers 5′-GGAATTCCATATGAAGCTTGGAGCTCATG-3′ and 5′-CGCGGATCCTCACCGCTTGGCCTCCACTCCTTCGTAC-GTG-3′. The PCR product was digested with both NdEI and BamHI and cloned in the pET-22b(+) vector linearized with the same enzymes. *trans*-Parinaric acid was supplied by Molecular Probes, Inc. (Eugene, OR). [^{14}C]Oleic acid was from Amersham Biosciences (Uppsala, Sweden). Clostripain (endoproteinase Arg-C), disuccinimidyl suberate, and buffers were purchased from Sigma-Aldrich (St. Louis, MO).

Ligands. In experiments involving holoproteins, a 10 mM solution of oleic acid in ethanol was added under stirring to the protein dissolved in buffer (2:1 fatty acid/protein molar ratio), and the mixture was incubated for at least 40 min at 37 °C. Oleic acid purity was ascertained by ^{1}H NMR spectroscopy in a Bruker MSL 300 spectrometer. *trans*-Parinaric acid concentration was estimated by ultraviolet absorption ($\epsilon_{306\ nm} = 77\ 000\ M^{-1}\ cm^{-1}$). The final concentration of ethanol in the assay never exceeded 1% (v/v).

Limited Proteolysis, Expression, and Purification of Δ98Δ. Clostripain (Arg-C, Sigma) was activated by incubation in 20 mM Tris-HCl, pH 8.0, and 1 mM DTT for 2 h prior to its use. Holo-IFABP was incubated with 1 mM DTT at the same temperature for at least 15 min before protease addition. To maximize the yield of Δ98Δ while reducing the appearance of lower molecular weight fragments, the optimal ratio of protein to protease was set to 200:1 (w/w). Digestion with this enzyme of holo-IFABP (0.5 mg/mL) dissolved in the same buffer was carried out at 30 °C for 1 h. To stop the digestion reaction, the mixture was dialyzed for 40 min at room temperature against the same buffer without DTT.

The dialyzed digestion mixture was centrifuged (at 16 100*g* for 10 min at room temperature), and the soluble material was sampled onto an ion-exchange chromatography column (Mono Q, Amersham Biosciences) previously equilibrated in 20 mM Tris-HCl, pH 8.0 (buffer A), at a flow rate of 1.0 mL/min. After washing out the unbound material, buffer A—with the addition of 0.1 M NaCl first or 1 M NaCl later—was used to elute peaks I and II, respectively. Fractions containing Δ98Δ were pooled together and dialyzed against buffer A.

On the other hand, purification of recombinant Δ98Δ was performed as follows. Cells were lysed by a combined treatment with lysozyme and DNAse I following an established protocol (*9*). Inclusion bodies were isolated by centrifugation (at 30 000*g* for 20 min at 4 °C) and washed with buffer B (50 mM Tris-HCl, 2 mM EDTA, and 100 mM NaCl, pH 8.0) added with urea up to 1 M concentration. After the sample was dissolved in buffer B containing urea up to 2 M concentration, the sample was further centrifuged (at 30 000*g* for 20 min at 4 °C) and the supernatant applied to a Superdex-75 column (Amersham Biosciences) equilibrated and eluted with buffer A.

To ascertain the identity and purity of proteins along the purification procedures, samples were mixed with sample buffer (0.005% (w/v) bromophenol blue; 4% (w/v) SDS; 10% (v/v) glycerol; 15% (v/v) 0.33 M Tris-HCl, pH 6.8; and 2% β-mercaptoethanol), heated for 3 min at 96 °C, and analyzed by Tris-Tricine SDS−PAGE (*10*). The composition of stacking and running gels was 4%T, 3%C and 16.5%T, 3%C, respectively. An initial voltage of 50 V was applied until the sample reached the running gel, then it was raised to 100 V for the remainder of the run. Gels were stained with 0.1% (w/v) colloidal Coomassie Brilliant Blue G dissolved in 2% (v/v) H_3PO_4 and 15% (w/v) $(NH_4)_2SO_4$ during 2 h and destained with distilled water. Digital images were processed with the Gel-Pro Analyzer Software (Media Cybernetics, Silver Spring, MD) using an *ad-hoc* filter to obtain densitometric data.

Reversed-Phase HPLC. Analytical reversed-phase HPLC was carried out on a Rainin Dynamax system equipped with a C4 column (214TP52, Vydac, Hesperia, CA). Elution of peptides and proteins was achieved with a linear gradient (0.05% aqueous TFA/0.05% TFA in acetonitrile, 100:0 to 20:80, v/v) developed for 80 min at a flow rate of 0.2 mL/min. Elution of peptidic material was monitored by measuring the absorbance at 215 nm.

Peptide Sequencing and Mass Spectrometry Analyses. Edman sequencing and amino acid analyses of peptides were carried out on Applied Biosystems 477 and Applied Biosystems 140A equipments, respectively, at the LANAIS-PRO facility (UBA-CONICET, Buenos Aires). MALDI-TOF analyses were run at the Protein/DNA Technology Center, Rockefeller University (New York, NY) through the kindness of Dr. T. P. King. ES Ion Trap-MS analyses were carried out in a Thermo-Finnigan LCQ-Duo with ion trap detector also installed at the LANAIS-PRO facility (UBA-CONICET, Buenos Aires).

Fourth-Derivative UV Spectra. Spectra were collected on a Jasco 7850 spectrophotometer, using a 1 cm path length cuvette sealed with a Teflon cap. IFABP or Δ98Δ (15−20 μM) dissolved in buffer A were used. Scans were recorded from 250 to 320 nm, with a bandwidth of 1 nm at a 40 nm/min speed. Data were taken every 0.2 nm. Fourth-derivative spectra were calculated by applying two successive cycles of second-order derivation: $\Delta^2A/\Delta\lambda^2 = (A_{i+20} - 2A_i + A_{i-20})/2\Delta\lambda^2$, as described elsewhere (*11*).

Fluorescence Measurements. Steady-state fluorescence measurements were performed in an Aminco Bowman Series 2 spectrofluorometer operating in the ratio mode and equipped with a thermostated cell holder connected to a circulating water bath set at 25 °C. A 1 cm path cuvette sealed with a Teflon cap was used. For *trans*-parinaric acid, excitation wavelength was 324 nm and emission was collected at 413 nm (a time trace of 7.5 s with sampling every 0.5 s). Spectral slit-widths were set to 4 and 16 nm, respectively. When the intrinsic fluorescence of proteins was measured, excitation wavelength was 295 nm and emission was collected in the range 310−400 nm. In this case, the spectral slit-widths were set to 4 nm for both monochromators. Data were corrected for dilution and inner filter effects

as indicated (*12*). For intrinsic fluorescence measurements, IFABP or Δ98Δ (15−20 μM) dissolved in buffer A was used. For each spectrum, either the wavelength of the center of mass (*13*), the intensity at the maximum of emission, or the total integrated intensity were the parameters used for further analysis.

Circular Dichroism. Spectra were recorded on a Jasco J-810 spectropolarimeter. Data in the near-UV (250−320 nm) or in the far-UV (200−250 nm) regions were collected using a 10 mm or a 1 mm path cuvettes, respectively. A scan speed of 20 nm/min with a time constant of 1 s was used for IFABP, while for Δ98Δ, scan speed was 5 nm/min with a time constant of 4 s. IFABP or Δ98Δ (15−25 μM) dissolved in buffer A was used. Each spectrum was measured at least three times, and the data were averaged to reduce noise. Molar ellipticity was calculated as described elsewhere, using mean residue weight values of 114.45 or 111.83 for IFABP or Δ98Δ, respectively (*14*).

Size-Exclusion Chromatography. Experiments were carried out in an FPLC system (Amersham Biosciences) with a Superdex-75 column equilibrated in 20 mM Tris-HCl, pH 8.0, with the addition of NaCl to the indicated concentrations. Elution profiles were recorded following the ultraviolet absorption at 280 nm. Stokes radii were calculated from a calibration curve of standard proteins according to Uversky (*15*).

Cross-Linking Experiments. A fresh solution of disuccinimidyl suberate (DSS) in dimethyl sulfoxide was added to protein samples (0.2 mg/mL in 20 mM sodium phosphate buffer, pH 8.0) to a final concentration of up to 10 μg/mL. The mixture was incubated for 1 h at 27 °C under continuous stirring. The reaction was stopped by adding an excess amount of Tris (1 μL of 200 mM Tris-HCl, pH 8.0, per 125 μL of mixture). After this, samples were dried in a Speed-Vac system (Savant, Farmingdale, NY) and analyzed by Tris-Tricine SDS−PAGE, as described above.

Equilibrium Unfolding Studies. Conformational transitions were monitored as a function of denaturant concentration by measuring the change in the intrinsic fluorescence intensity of the proteins. GdnHCl stock solutions were prepared on the day of the experiment. Individual samples ranging in denaturant concentration from 0 to 3 M GdnHCl were obtained by dilution of a fixed volume of a stock solution of protein in mixtures of 20 mM Tris-HCl buffer, 100 mM NaCl, pH 8.0, buffer and 8 M GdnHCl (4 μM final protein concentration). Following incubation for at least 1 h to ensure that the equilibrium had been reached, samples were analyzed. Fluorescence data were corrected for the background signal of buffer and denaturant and expressed in relative units to equate protein species with different intrinsic fluorescence. Nonlinear least-squares fits to the equilibrium data were achieved using an equation representing a two-state model for protein denaturation adapted from Santoro and Bolem (*16*).

Binding Experiments. 1. Binding to Oleic Acid. The binding of this ligand was monitored by measuring changes in the intensity of intrinsic fluorescence of the proteins. For this assay, the concentration of both proteins was 2 μM. The ligand was repeatedly added to each protein dissolved in buffer A and to buffer A alone (blank). Incubation for 2 min at 25 °C ensured complete equilibration. Nonlinear regression fitting to the binding data was achieved with an equation corresponding to a model of two nonidentical, noninteracting sites using the Microsoft Excel solver tool. Data were corrected for the decrease in fluorescence emission due to the presence of different amounts of ethanol. In no case the final concentration of ethanol exceeded 2% (v/v).

2. Binding to Parinaric Acid. The binding of this fatty acid was monitored by the enhancement of fluorescence observed for the bound ligand. For this assay, the concentration of both proteins was 0.5 μM. The ligand was repeatedly added to each protein dissolved in buffer A and to buffer A alone (blank). Incubation for 3 min at 25 °C ensured complete equilibration. Nonlinear regression fitting to the binding data was done as described above. Due to the strong absorption of the fatty acid, data were corrected for inner filter effect. Final concentration of ethanol never exceeded 2% (v/v).

Distance Maps, Neighborhood, and Surface Analyses. A C_α atoms file was generated from the pdb file of IFABP (code 2IFB). A Microsoft Excel macro was written (i) to calculate all pairwise distances between C_α centers, (ii) to sort those distances by comparison with a preset length, and (iii) to represent data in a graphical fashion. Data were plotted as (i) a classical two-dimensional dot matrix map of contours at a given boundary distance (typically 8 or 20 Å) and (ii) a one-dimensional plot representing the number of neighboring C_α carbons as a function of the position in the amino acid sequence.

The Surface Racer program (version 1.1, (*17*)) was used to calculate solvent accessible surface areas, with the choice of the F. M. Richards' van der Waals radii set and a 1.4 Å probe radius for the water molecule. A modification of the source code of the program was implemented to allow for the automatic calculation of both nonpolar and total accessible surface areas on sets of edited pdb files. These were in turn generated by removal of sequential fragments of seven or nine amino acid residues (seven or nine residue windows) from the original pdb file 2IFB.

RESULTS

Production and Purification of Δ98Δ. It has been previously shown that apo-IFABP is much more sensitive toward protease digestion than holo-IFABP (*7*). Partial digestion of holo-IFABP with clostripain generates an 11 kDa fragment which is resistant to further proteolysis. This process was optimized in terms of time and enzyme/substrate ratio so as to enhance the production of that fragment while minimizing additional degradation (Figure 1A). The time course of proteolysis of holo-IFABP follows a biphasic curve which mirrors the appearance of the 11 kDa fragment. Smaller peptides, as evidenced by SDS−PAGE, appear at a much lower rate. Similarly, a biphasic behavior is also evident for the appearance of N-terminal peptides after C4 RP-HPLC analysis (Figure 1B). In particular, this holds true for the intact N-terminal fragment, pointing to a common initial cleavage event giving rise to this peptide and to the 11 kDa fragment.

The latter polypeptide was purified in a single step by anion exchange chromatography (peak II in Figure 2). IFABP has six potential sites for the action of clostripain: R10, R28, R56, R95, R106, and R126. However, Edman degradation of peak II rendered a unique sequence (KLGAH), indicating

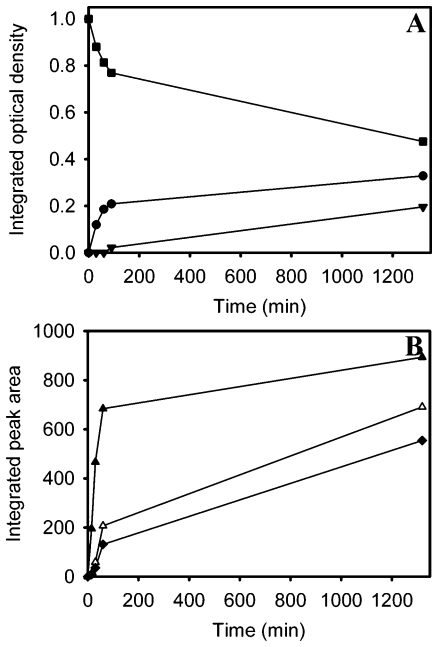

FIGURE 1: Kinetics of proteolysis of holo-IFABP by clostripain. (A) The integrated optical density of bands stained by colloidal Coomassie Blue after SDS−PAGE is plotted: IFABP (■), the 11 kDa fragment (●), and low molecular weight fragments (▼). (B) The integrated peak areas of fragments derived from the N-terminus separated by C4 RP-HPLC: 1−10 (◆), 11−28 (△), and 1−28 + 11−28 (▲).

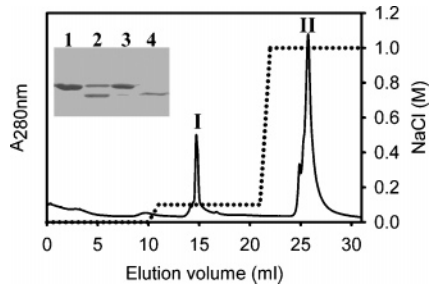

FIGURE 2: Elution profile of the digestion mixture of holo-IFABP by clostripain after anion exchange chromatography (Mono Q). The inset shows an SDS−PAGE analysis of each fraction: the pass-through material (lane 1), peak I (lane 2), the full digestion mixture (lane 3), and peak II (lane 4).

cleavage at R28, a residue belonging to helix αII. In addition, the mass of this peptide measured by MALDI-TOF spectrometry was 10 958.8 Da. Taken together, it can be concluded that the 11 kDa fragment (henceforth named Δ98Δ) spans from K29 to R126, thus, encompassing 98 amino acids and lacking both the N- and C-termini of the parent protein (Figure 3). We note that in IFABP the closure of the β-barrel is achieved by hydrogen-bonding contacts between residues of the distal part of strands βA and βJ, which are absent in Δ98Δ. On the other hand, Δ98Δ preserves all residues involved in the hydrophobic collapse (Figure 4), the earliest event in IFABP folding, that is, F47, F62, L64, F68, W82, M84, and L89 (*18*).

One issue worth considering at this stage was assessing the status (apo or holo form) of the protein obtained in this fashion. To this end, a sample of IFABP loaded with [^{14}C]-oleic acid was enzymatically digested and purified as usual by anion exchange chromatography (Mono Q). Monitoring the radioactivity in the eluate indicated that fatty acids are retained by the column and only later eluted with 75% aqueous acetic acid (data not shown). Indeed, no detectable coelution of the ligand occurs with protein peak II. Thus, this procedure renders Δ98Δ in its apo form.

Furthermore, to explore the possibility of Δ98Δ forming a noncovalent complex in solution with the removed smaller fragments, the composition of the protein eluting in peak II was compared to the full digestion mixture. For this purpose, we employed a combination of reversed-phase chromatography (RP-HPLC), amino acid analysis, Edman sequencing, and mass spectrometry. The elution profile of the full digestion mixture separated in a C4 RP-HPLC shows a complex pattern dominated by a major peak (Figure 5B), whereas peak II presents a single peak (Figure 5A). Peak A in Figure 5B was identified as peptide 1−10 by amino acid analysis. Peak B is peptide 11−28, as judged by its average mass of 2228.7 Da and its N-terminal sequence (NENYExFM). Peak C represents a mixture of peptides 11−28 (N-terminal sequence NENYExFMEKMG) and 1−28 (3406.4 Da), while intact IFABP and Δ98Δ elute as the poorly resolved peaks D and E. Most significantly, the elution profile of peak II treated with 4 M GdnHCl reveals a single peak in RP-HPLC at the same percentage of acetonitrile as peak E. Since no peak appears corresponding to any other proteolytic fragment found in the full digestion mixture, it can be inferred that Δ98Δ is a single polypeptide. Moreover, Edman sequencing of Δ98Δ purified in this fashion renders a unique result (KLGAH), thus, eliminating the possibility of a putative noncovalent complex.

To fulfill the requirements of available mass for a full structural analysis, we also undertook the cloning and overexpression of Δ98Δ and its purification from inclusion bodies. Solubilization of this material in the presence of 2 M urea and elution through Superdex-75 sufficed to yield this fragment in pure form (data not shown). This cloned variant differs from that obtained by digestion by the presence of an additional M residue at the N-terminus (11 089 Da).

Fourth-Derivative UV Spectra. The environment of the aromatic residues of Δ98Δ and IFABP was studied by UV absorption spectroscopy. For this purpose, we applied fourth-derivative analysis, a sensitive technique previously employed to assess the conformation of several proteins, including IFABP (*6*, *8*). The main advantages of this method have been pointed out by Butler (*19*): (i) the maxima of the fourth-derivative curves are located almost at the same positions than those of the original zero-order spectrum; (ii) the technique can reveal the presence of constituent bands that are not apparent in the original spectrum; and (iii) the amplitude of the fourth-derivative curve shows an inverse fourth-power dependence on the half-width of the original band, thus, enhancing the narrow bands.

Although Δ98Δ only conserves 3 out of 4 Y, 5 out of 8 F, and 1 out of 2 W residues, overall, the fourth-derivative spectra of both IFABP and Δ98Δ show a similar fine structure, suggesting a common environment for their aromatic residues (Figure 6). Characteristic wavelengths corresponding to the electronic transitions of Y and W (λ_2 and λ_3) in Δ98Δ are centered at the same positions as those found for the native full-length protein. The only significant difference observed for Δ98Δ is a decrease in the amplitude of bands above 285 nm. This change can be attributed to the absence of W6, which leads to a broadening in the zero-

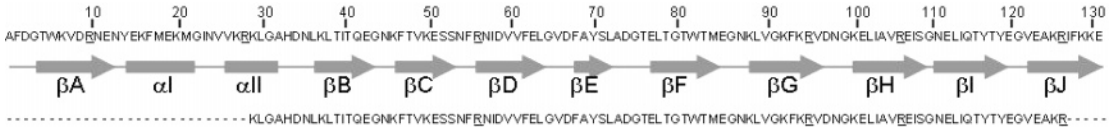

FIGURE 3: Amino acid sequences of IFABP and Δ98Δ. A schematic representation of the secondary structure elements of IFABP is shown alongside.

FIGURE 4: Ribbon structure of IFABP (PDB 2IFB) where the Δ98Δ construct is indicated. The excised N- and C-termini are shown in black, Δ98Δ is colored gray, and residues belonging to the hydrophobic core are depicted with their side chains in poly-tube representation colored black.

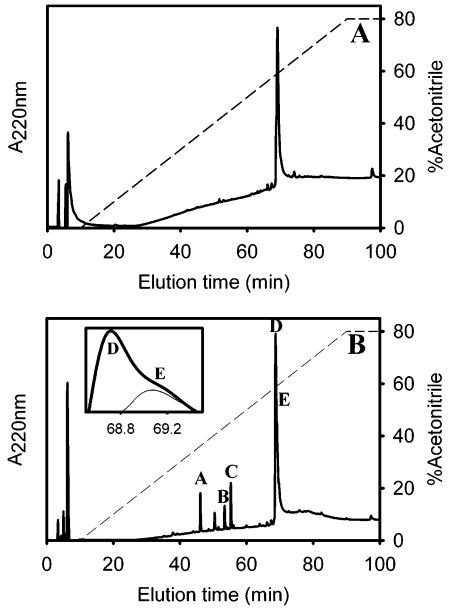

FIGURE 5: Elution profile of purified Δ98Δ as compared to the full digestion mixture after C4 RP-HPLC. Peak II (Figure 2) was rechromatographed, and results (panel A) are shown above a similar analysis of the sample originally loaded onto the Mono Q column (panel B). The inset shows the superimposition of a selected region of each profile. Labeled peaks correspond to peptides identified and mentioned in the main text.

order spectrum. Indeed, previous work with mutant IFABPs having either W6 (IFABP^{W82}) or W82 (IFABP^{W6}) replaced by F has identified W6 as the main contributor to the 285 nm signal (*20*). Finally, oleic acid binding does not cause any noticeable spectral change for either Δ98Δ or IFABP (holo vs apo forms).

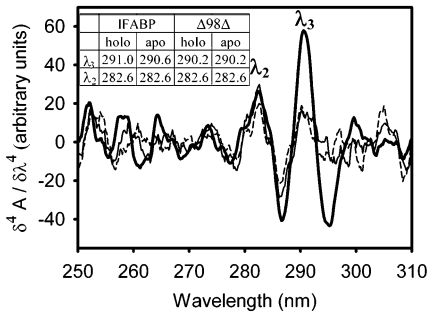

FIGURE 6: Fourth-derivative absorption spectra of apo-IFABP (—), apo-Δ98Δ (−), and holo-Δ98Δ (---). The holo-IFABP spectrum is not displayed because it superimposes exactly over that of apo-IFABP. A table with the values of characteristic wavelengths is shown as an inset.

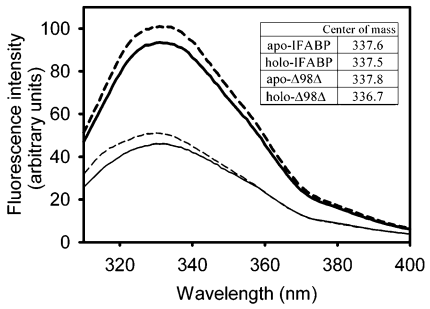

FIGURE 7: Fluorescence emission spectra of apo-IFABP (—), holo-IFABP (---), apo-Δ98Δ (−), and holo-Δ98Δ (---). The wavelengths of the center of mass are shown as an inset.

Fluorescence Spectroscopy. The center of mass of the spectra of apo-Δ98Δ is typical of a W residue located in a hydrophobic environment (337.6 nm) and is minimally red-shifted (0.2 nm) as compared to apo-IFABP (Figure 7). Binding of oleic acid causes a slight increase in the intensity and a blue shift of the center of mass of both proteins (inset to Figure 7). This behavior can be readily explained after examining the location of the fluorophore. W82 is deeply buried in the hydrophobic core and surrounded by an array of benzyl rings (F2, F47, F62, F68, and F93) and aliphatic side chains (L64, M84, and L89). Although not accessible to the external solvent, in apo-IFABP, W82 contacts two internal water molecules and the guanidinium moiety of R106 (*20*). Upon ligand binding, this charged group forms an ion bridge with the carboxylate of the ligand fatty acid, while water contacts are lost, thus, explaining the blue shift observed for the holo forms.

The fluorescence intensity of Δ98Δ is approximately one-half of that observed for IFABP. At least two reasons might account for this fact. One should bear in mind that W82, the only W residue remaining in Δ98Δ, has been recognized as the main contributor to fluorescence. In this regard, mutant IFABP^{W82} lacking W6 (see above) yields 65% of the fluorescence intensity as compared to the wild-type protein (E. M. Clérico and M. R. Ermácora, University of Quilmes, Argentina, unpublished results). Therefore, removal of W6 might not fully account for the observed decrease in

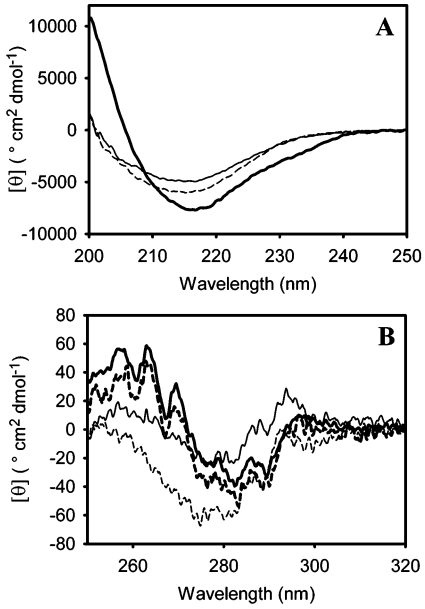

FIGURE 8: Circular dichroism spectra of Δ98Δ and IFABP. The (A) far-UV and (B) near-UV CD spectra are shown: apo-IFABP (—), holo-IFABP (---), apo-Δ98Δ (−), and holo-Δ98Δ (---).

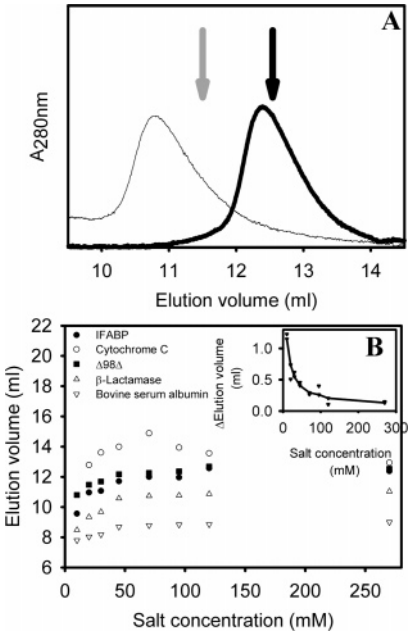

FIGURE 9: Size-exclusion chromatography of Δ98Δ compared to IFABP and other proteins. (A) Δ98Δ was sampled onto a Superdex-75 column and eluted at low (−) and high (—) ionic strength. Arrows indicate the elution volumes of IFABP under the same conditions (low and high ionic strength in gray and black, respectively). (B) The effect of increasing salt concentration on the elution volume of these and other proteins. The inset shows the difference between the elution volume of Δ98Δ and IFABP (ΔElution volume) as a function of ionic strength.

fluorescence intensity. In addition, minimal perturbations to the tight aromatic environment around W82 and/or an increased solvent quenching effect in Δ98Δ (expected from a facilitated solvent access to the binding pocket) might also contribute to the changes observed.

Circular Dichroism. The far-UV circular dichroism (CD) spectra of apo- and holo-Δ98Δ show minima at approximately 216 nm, a characteristic feature of β-sheet proteins. A similar result is observed for IFABP, regardless of the presence of oleic acid (Figure 8A). Nevertheless, the absolute ellipticity value of apo-Δ98Δ is about 65% that of apo-IFABP. At variance with the full protein, when oleic acid is bound to Δ98Δ, a 20% increase in the absolute value of the signal at 216 nm is observed. This behavior could be attributed to a ligand-induced ordering effect. In fact, if the holo forms of both proteins are compared, the difference between the amplitudes becomes smaller (about 20%). Indeed, a simple theoretical quantitative analysis assuming a structure for Δ98Δ preserving the secondary structure features of IFABP yields an expected 20% decrease in the signal at 216 nm.

Two features of the spectrum of IFABP are conspicuously absent in Δ98Δ: (i) the positive band centered at 200 nm and (ii) the shoulder at around 230 nm. Most prominently, the absence of the 200 nm band and the diminished intensity at 216 nm in Δ98Δ could be mainly attributed to the absence of the helical domain, whose contribution to ellipticity is almost twice that of a β-sheet on a molar basis (*21*) and, to a lesser extent, to the expected reduction in the β-sheet content due to the absence of the first strand. Although secondary structure elements are the main contributors to far-UV CD, in many instances, aromatic residues add signal to this region as well (*22*). For IFABP, it has been described that W6 contributes two negative bands at 202 and 225 nm (*20*), thus, explaining the missing shoulder at around 230 nm in the abridged form.

Near-UV CD is a very sensitive tool to follow changes in the environment around aromatic residues. Remarkably, the presence of a structured spectrum in this region (Figure 8B) emphasizes the fact that Δ98Δ adopts a folded state showing similarities with that of the native protein and quite distinct from a classical molten globule (*23*). In this regard, the fine structures of the spectra above 280 nm of Δ98Δ and IFABP are quite similar, indicating that W82 is placed in a similar milieu in both proteins. However, Δ98Δ presents a weaker signal in the range 250−270 nm as compared to IFABP. More precisely, loss of fine structure and reduced magnitude of the bands occur. This region could be assigned, in principle, to the dichroic absorption of F residues, although H residues could contribute as well. The changes observed could arise from the loss of F residues 2, 17, and 128 in Δ98Δ and/or from slightly reduced asymmetry around the remaining F residues. We notice that these changes occur in a spectral region where IFABP shows extreme temperature dependence well below the denaturation temperature (*8*). Upon oleic acid binding, the magnitude of the spectral signals of Δ98Δ is enhanced, suggesting the ligand induces a more ordered structure. This behavior is not uncommon and is consistent with that observed in the far-UV region. A similar, but much less intense, effect is also observed for IFABP.

Aggregation State and Compactness. The hydrodynamic properties of Δ98Δ were studied by size-exclusion chromatography and compared with those of intact IFABP. The elution profiles of Δ98Δ at 0 and 100 mM NaCl added to the buffer are shown in Figure 9A, where arrows indicate the elution positions of IFABP under the same conditions. Despite being 4 kDa smaller than IFABP, the Stokes radius (R_s) of Δ98Δ at 100 mM NaCl (20.1 ± 0.7 Å) is almost identical to that of IFABP (20.0 ± 0.5 Å) and 16% larger than the predicted value for a globular protein of the same molecular weight (17.3 Å). Taken together, these data are

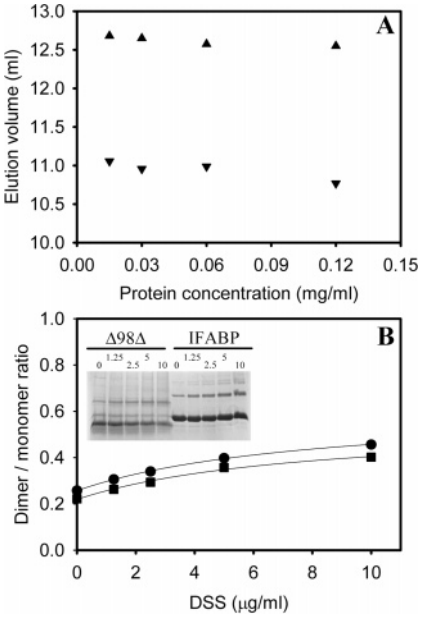

FIGURE 10: (A) Size-exclusion chromatography of Δ98Δ as a function of protein concentration. The behavior of Δ98Δ sampled at low (▼) and high (▲) ionic strength is shown. (B) Results from cross-linking experiments with DSS of both Δ98Δ (●) and IFABP (■). The dimer/monomer ratio is plotted as a function of reagent concentration. The inset shows the separation of covalent products in each case by SDS−PAGE. Numbers on lanes indicate the DSS concentration in micrograms per milliliter.

consistent with Δ98Δ adopting a monomeric, but slightly expanded, conformational state. However, at low ionic strength, an anomalous behavior is observed. The R_s measured for Δ98Δ (21.8 ± 0.7 Å) is 9% larger than that of IFABP (20.0 ± 1.2 Å). To assess whether the striking differences observed are characteristic of this class of proteins or a phenomenon common to many proteins, we undertook the following experiment. The chromatographic behavior of several proteins, including IFABP and Δ98Δ, was studied at different salt concentrations (Figure 9B). As expected, no significant change in the elution volume of any protein assayed was observed above 100 mM NaCl. Interestingly, for all proteins below 55 mM NaCl, this parameter decreases as salt concentration is reduced. This behavior is probably due to the interaction of the polypeptide chain with the small number of negatively charged groups present in the column matrix. To explain the larger difference observed between Δ98Δ and IFABP at low salt concentration, one could invoke that Δ98Δ (pI 5.4, as measured by isoelectric focusing), being more negatively charged than IFABP (pI 6.9, also measured by isoelectric focusing), would be more strongly repelled by the matrix (inset to Figure 9B).

Despite the anomaly pointed out above, the R_s value of Δ98Δ (21.8 Å) at low ionic strength would match the size of a globular protein with a molecular weight corresponding to that of a hypothetical dimer. To disprove this contention, the following experiments were carried out. When sampling Δ98Δ in a low range of protein concentration, a single peak with identical retention volume was consistently obtained at each ionic strength assayed (10.9 ± 0.3 and 12.6 ± 0.2 mL for 0 and 100 mM NaCl, respectively, Figure 10A), a behavior that is in disagreement with the dissociation expected for a putative dimer. To confirm this last point, chemical cross-linking experiments were also performed

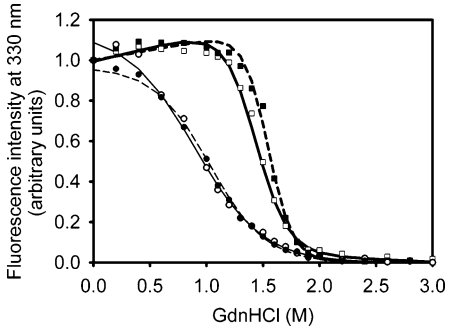

FIGURE 11: Equilibrium unfolding transitions of Δ98Δ and IFABP monitored by the change in fluorescence intensity: apo-IFABP (□), holo-IFABP (■), apo-Δ98Δ (○), and holo-Δ98Δ (●).

using disuccinimidyl suberate (DSS), an amine-reactive homobifuntional reagent (Figure 10B). Remarkably, under identical experimental conditions and over a range of cross-linker concentrations, the fragment and the full-length protein exhibit the same minimal propensity to cross-link. Since IFABP is well-known to behave as a monomer, a fact confirmed by a light-scattering experiment (which yielded a value of 14 750 Da), the evidence would support that Δ98Δ is also a monomer.

Equilibrium Unfolding Transition. Most significantly, the unfolding of the abridged variant Δ98Δ shows a cooperative transition (Figure 11). The free energies of unfolding for apo- and holo-Δ98Δ are $\Delta G^\circ_{H_2O} = 1.73$ kcal mol^{-1} ($m = 1.93$ kcal mol^{-1} M^{-1}) and 2.45 kcal mol^{-1} ($m = 2.37$ kcal mol^{-1} M^{-1}), corresponding to transition midpoints of 0.90 and 1.03 M GdnHCl, respectively. By comparison, IFABP unfolds through a cooperative transition centered at 1.43 M GdnHCl, with a $\Delta G^\circ_{H_2O}$ of 5.87 kcal mol^{-1} ($m = 4.11$ kcal mol^{-1} M^{-1}), while oleic acid binding causes further stabilization ($\Delta G^\circ_{H_2O} = 8.21$ kcal mol^{-1}, $m = 5.32$ kcal mol^{-1} M^{-1}). The latter results are in good agreement with previous reports for the full-length protein (*2*). Although oleic acid binding slightly enhances the stability of Δ98Δ, the effect does not appear to be as important as in IFABP. This difference likely arises as a consequence of the lesser affinity of the truncated variant toward the ligand (see below).

Furthermore, it is noteworthy to compare our variant with other truncated constructs of IFABP. Strikingly, a protein lacking only the three C-terminal residues is reported to have very similar unfolding parameters ($IFABP_{1-128}$, $\Delta G^\circ_{H_2O}$ of 2.57 kcal mol^{-1}, (*6*)). On the other hand, although Δ17-SG and Δ27-GG are reported to be more stable than Δ98Δ, their transition midpoints lie in the same range of GdnHCl concentrations (0.86 and 1.13 M, respectively, (*5*)).

Binding Activity. Fatty acid binding to Δ98Δ and IFABP was assayed as follows. Oleic acid binding was monitored by changes in the steady-state tryptophan fluorescence emission of the protein, whereas *trans*-parinaric acid allows binding to be measured by changes in the fluorescence emission of the probe itself (Figure 12). Values for the dissociation constants (K_d) were obtained by fitting to the data an equation corresponding to a binding model considering two sites. Both protein species present a binding phase of high affinity followed by a low-affinity one. Although showing lower affinity for oleic acid than IFABP ($K_d = 1.0$ μM), Δ98Δ retains the ability to bind this ligand ($K_d = 5.1$ μM). On the other hand, both proteins show an enhanced

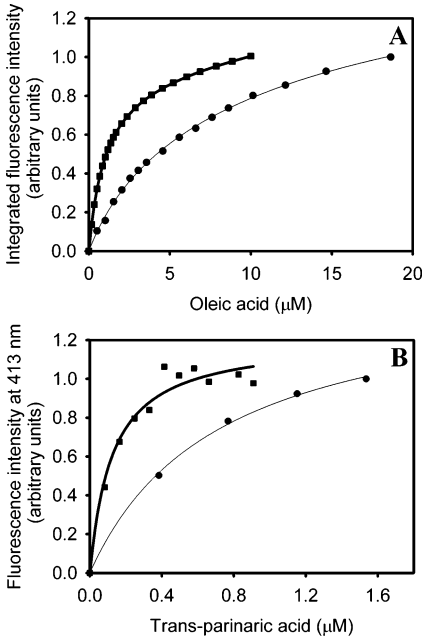

FIGURE 12: Fatty acid binding activity of Δ98Δ and IFABP. (A) Binding isotherms for oleic acid evidenced by the change in the intrinsic fluorescence emission of the proteins. (B) Binding of the fluorescent probe *trans*-parinaric acid is shown: IFABP (■) and Δ98Δ (●).

affinity for *trans*-parinaric acid (K_d = 0.13 and 0.72 μM for IFABP and Δ98Δ, respectively). Consistently, for both ligand fatty acids, the affinity demonstrated by Δ98Δ is about 5-fold less than that shown by IFABP.

Similarly to our variant, a K_d of 4−5 μM toward oleic acid is reported for Δ17-SG. NMR studies of this helix-less variant revealed that the interaction with the carboxylate end of the fatty acid is similar to that observed for IFABP. Clearly, the loss in affinity arises from the lack of the α-helical domain. In addition, the kinetics of binding indicates that the association rates for oleic acid in Δ17-SG and IFABP are similar, while the dissociation rate is slower for the latter (*24*). Recently, on the basis of oleate-binding isotherms, it has been shown that Δ27-GG might bind more than three fatty acid molecules, whereas Δ17-SG and IFABP would only bind two ligand molecules, albeit the second one with very low affinity (*5*). However, in the absence of any further structural information, the precise location of the second site remains unclear.

A clear link can be established between conformational and binding equilibria. Regardless of the complexities associated with the conformational states of IFABP coexisting in solution (*8*), one can in principle postulate (i) a two-state unfolding transition and (ii) the ligand binding solely to the native state N. Under these assumptions, the apparent standard free-energy difference for the conformational transition ($\Delta G°_{app}$, that measured for the holo form) relates to the true free-energy difference ($\Delta G°$, that measured for the apo form) by the following equation:

$$\Delta\Delta G° = \Delta G°_{app} - \Delta G° = RT \ln(1 + [L]/K_d)$$

where K_d denotes the dissociation constant for the binding equilibrium reported above and [L] is the concentration of free ligand in equilibrium with the holo form. Indeed, for oleic acid binding to IFABP or Δ98Δ (at a 16 μM ligand concentration), the measured $\Delta\Delta G°$ values are 2.34 or 0.72 kcal/mol, in general agreement with the predictions (RT ln-$(1 + [L]/K_d)$ equals 1.68 or 0.84 kcal/mol, respectively).

Distance Maps, Neighborhood, and Surface Analyses. To examine the topological consequences of excising the fragments absent in Δ98Δ, we undertook a geometrical analysis upon the coordinates of IFABP. The local density within the protein was estimated by counting the number of C_α atoms located inside a sphere centered at each C_α carbon along the amino acid sequence. For this purpose, the number and quality of neighbors around a particular residue were calculated using spheres of 20 and 8 Å radii, respectively. The latter produced a map in which amino acid proximity was plotted (Figure 13A). A widening in the diagonal is evident at the helix-turn-helix motif, while the hydrogen-bonding network between antiparallel β-strands appears as lines perpendicular to the diagonal. In this graph, anomalous β-contacts show up as missing (βD−βE) or truncated segments, as it is evident for the pairs βA−βB and βA−βJ. The closure of the barrel at one edge of the β-clam involves the twisting of strand A to allow contact with its neighbors. Thus, the N-terminal end of strand A contacts strand B, while the C-terminal end interacts with strand J. For the βD−βE pair, the interaction between these strands is through side-chain atoms or bridging water molecules that serve to fill the gap (*3*). Remarkably, Δ98Δ is devoid precisely of both partners postulated to maintain the integrity of the barrel, that is, the whole of β-strand A and the end of β-strand J.

In Figure 13B the number of C_α neighbors around each amino acid is represented. A sphere of 20 Å radius proved to be the most discriminating to evaluate the local density around each residue (result not shown). Here, it becomes evident that peptides 1−28 and 127−131 encompass a region with the least number of neighboring residues in the whole protein (at most, 82 C_α neighbors for Y14 and 88 for I127). By comparison, those strands including amino acids spatially close to the core region exhibit a higher number of neighbors (e.g., 119 for Q115, belonging to strand I). Moreover, on average, the number of neighbors for peptides 1−28 and 127−131 is 69 and 68, respectively, significantly smaller than that for the sequence 29−126 (77 C_α neighbors).

A surface analysis involving the calculation of both the nonpolar and the total accessible surface areas (Figure 13, panels C and D, respectively) sheds light on the consequences of excising the peptides absent in Δ98Δ. For this purpose, we devised an automated procedure which systematically removes from the original pdb file peptides of a desired length (seven or nine residue windows) along the amino acid sequence. For each edited file, both the nonpolar and the total accessible surface area were calculated with Surface Racer (*17*). Interestingly, the removal of peptide 1−28 does not appear to expose so much new nonpolar area, as is the case for most of the β-stands of the barrel lining the hydrophobic core (with the exception of strands D and E, which constitute the opposite edge of the β-clam). Finally, a similar analysis run with the total area as the parameter plotted also yield the lowest peaks for the regions including β-strands A, D, and E, pointing to the high convexity of those sections of the protein.

These results numerically depict the fact that IFABP is an oblate where peptides 1−28 and 127−131 are placed at

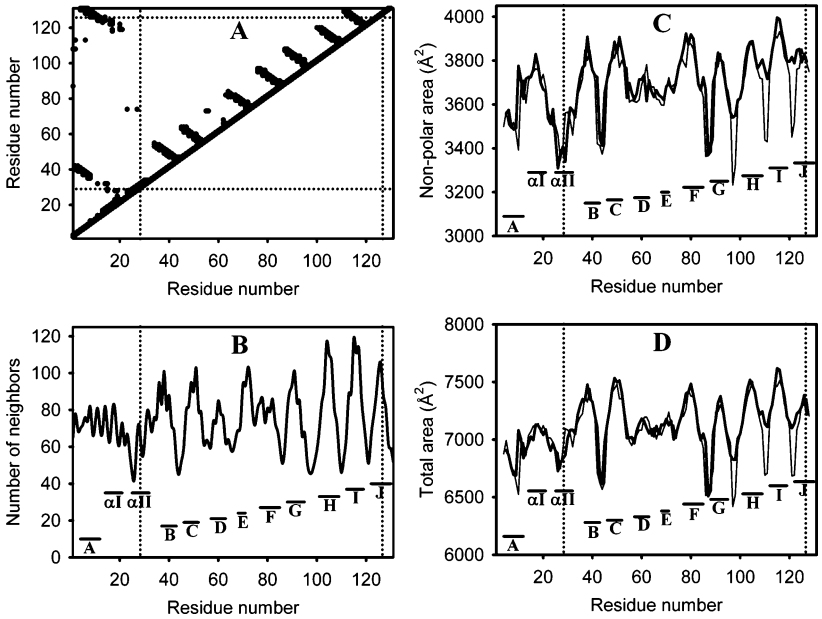

FIGURE 13: (A) Two-dimensional map of IFABP showing pairwise distances within 8 Å. (B) Distance profile of IFABP: the number of neighbors (C_α carbons) within a 20 Å distance is plotted against residue number. The solid bars represent the secondary structure elements. (C and D) Plots of the nonpolar (C) and total area (D) calculated by removal of hepta- (−) or nona-peptides (—) along the amino acid sequence. Dashed lines are shown at the beginning and end of Δ98Δ.

a peripheral position, along a distal edge located opposite to the compact hydrophobic core (Figure 4).

DISCUSSION

The ultimate aim of this work is to draw critical features determining the folding and function of the β-barrel motif protein IFABP. For this purpose, protein truncation provided the means to selectively isolate a stable fragment complying with those requirements. In this regard, Δ98Δ is the result of a major deletion of the parent protein and constitutes the shortest form described so far preserving binding activity. Interestingly, one could learn from this model about the consequences of removing not only a peripheral helix-turn-helix motif but also strands compromised in the closure of the β-barrel.

Δ98Δ was obtained either in its recombinant form or by limited proteolysis of holo-IFABP with clostripain. This 11 kDa fragment lacks the N-terminal 1−28 stretch and the last five amino acids belonging to the C-terminus. Protein truncation has been extensively used to populate nonnative states under physiological conditions (*25*, *26*). In particular, an abridged form of IFABP ($IFABP_{1-128}$) was generated by deleting the last three C-terminal residues (*6*). The rationale behind this approach was that by removing those residues the β-barrel would open, thus, leaving the two sheets free to slide against each other and allowing free rotation of the side chains at the internal interface. The resulting protein is a monomeric and compact nonnative state of IFABP, which is highly susceptible to proteolytic attack, and its unfolding behavior clearly indicates a loose tertiary structure. An important difference between $IFABP_{1-128}$ and Δ98Δ is that the latter is devoid of both stretches responsible for the closure of the β-barrel.

The role of βA−βJ contacts in maintaining the integrity of the β-barrel can be drawn from the results obtained with two helix-less variants of IFABP (*4*, *5*, *27*). The first one (Δ17-SG) was generated by deleting residues 15−31 and inserting an SG linker between strands A and B. NMR analysis of this protein showed that its β-strand topology is nearly identical to that of IFABP, confirming that the helical domain is not essential to stabilize the β-sheet domain. There are two main differences between Δ17-SG and IFABP. First, because of the large opening generated, Δ17-SG resembles a teacup rather than a clamshell. Second, the distal portion of the β-strand A, that adjacent to the deletion site, is unstructured in Δ17-SG as a consequence of the linking loop being longer than anticipated (spanning from residues 9 to 20 in the variant). A second generation of helix-less IFABP (Δ27-GG) was engineered by removing 27 residues (from residues 9 to 35) and inserting instead a GG linker. Despite its short size, the overall topology of Δ27-GG is similar to that of Δ17-SG and IFABP. Both generations of helix-less IFABPs lack bonds between strands A and J, leaving the β-barrel without its closure. Interestingly, these findings show that removing βA−βJ contacts does not necessary lead to an opening of the β-barrel.

In our case, although conserving only 75% of the 131 residues of IFABP, Δ98Δ remains stable in solution even in the absence of the ligand fatty acid. The possibility of Δ98Δ being a noncovalent complex with the excised N-terminal peptide was rejected, because the main fragment elutes as a single peak after C4 RP-HPLC and shows a unique N-terminal amino acid sequence.

A body of evidence derived form optical spectroscopies supports the fact that Δ98Δ bears a stable well-folded state. The fine structure of the fourth-derivative UV spectra revealed that Δ98Δ has its unique tryptophan placed in a similar milieu to that of IFABP. Moreover, the features of fluorescence emission of Δ98Δ and the full-length protein confirm the view of a common buried environment for the conserved W. A hint regarding the binding function of the fragment arises from the fact that a blue shift of the center of mass of fluorescence occurs upon addition of oleic acid. This effect is likely the consequence of the proximity of the

carboxylate group of the fatty acid to the guanidinium side chain of R106, which disrupts the contacts of W82 with R106 and two fixed waters (*28*). On the other hand, the decrease in fluorescence intensity can be accounted for mostly by the loss of W6.

The far-UV CD spectrum of Δ98Δ is typical of a β-sheet protein but shows a 35% decrease in intensity as compared to IFABP. This change is mainly due to the absence of the α-helical moiety and the loss of several aromatic residues, most prominently W6. Unlike the helix-less versions of IFABP, in which only the distal part of strand A is absent or unstructured, Δ98Δ lacks the entire strand A and the N-terminal end of strand J. Remarkably, this new species appears to preserve the integrity of the tertiary structure, as revealed by near-UV CD spectra. Upon ligand binding, Δ98Δ undergoes further stabilization, a fact substantiated by the increase in ellipticity in both near- and far-UV CD regions. On the other hand, size-exclusion chromatography revealed that Δ98Δ, despite being 4 kDa smaller than IFABP, has a similar R_s, suggesting a slightly less compact structure.

Unlike other truncated forms of IFABP, Δ98Δ has only one W residue. The side chain of this amino acid is buried within the hydrophobic core and becomes useful as a local probe to follow conformational changes. Surprisingly, although Δ98Δ is devoid of 12% of native contacts (see map at 8 Å distance, Figure 13A), it unfolds through a cooperative transition. Its stability is similar to that of $IFABP_{1-128}$ but smaller compared to that of full-length IFABP or any of the two helix-less variants. The underlying reasons for the low stability of $IFABP_{1-128}$ are still not known (*6*). On the other hand, Δ27-GG is less stable than the wild-type protein, possibly due to the loss of inter domain hydrogen bonds and van der Waals contacts between the α-helical and β-sheet domains, but it is more stable than Δ17-SG, which has a longer unstructured loop (*5*). A common motif in all these constructs is the preservation of the key structural determinants of the hydrophobic core. We believe that a delicate balance exists between two opposing driving forces leading to the overall stability of a given variant, that is, the intrinsic cohesion provided by a compact well-folded core versus the added entropy and loss of interstrand hydrogen bonds associated to an increased mobility of the β-strands and loops of the barrel. In this scenario, Δ98Δ might play with advantage by comparison with Δ17-SG or $IFABP_{1-128}$, due to the absence of the N-terminal moiety.

Δ98Δ has been cloned and overexpressed in *E. coli*. The large amount of protein produced causes it to appear almost exclusively in inclusion bodies. To purify this abridged variant, this material was dissolved in buffer containing 2 M urea, a concentration lower than that needed to unfold Δ98Δ (data not shown). In all respects, the recombinant species behaves identically to the fragment obtained from proteolysis, a fact consistent with the hierarchical folding mechanism proposed for IFABP (*18*). In accordance with this model, the unfolded polypeptide first collapses into a semicompact structure surrounding a hydrophobic core consisting of F47, F62, L64, F68, W82, M84, and L89. Next, β-strands B and G propagate outwardly from the hydrophobic core, establishing the native topology. Finally, this scaffold serves as a template to fold the last three β-strands (H−J), completing the native hydrogen-bonding network. The formation of the native structure depends on the coordinated interaction between both halves of the protein. It has been argued that peptides of IFABP composed of either half of the clamshell would not form a β-sheet structure. Since Δ98Δ encompasses a sequence which corresponds to a continuous stretch of the parent protein beginning at strand βB and ending at the N-terminal half of strand βJ, it might fold through a similar hierarchical way as well. This process might lead to a native-like topology with a compact hydrophobic core but endowed with an expanded periphery. Moreover, the ability of Δ98Δ to bind fatty acids with affinities similar to those of the helix-less variants and IFABP suggests a conserved structure able to provide a suitable environment for binding.

In summary, although Δ98Δ lacks one-quarter of the sequence of the parent protein, it is a stable, monomeric, and functional truncated form of IFABP. The reasons for this remarkable behavior lie in the ancillary role played by the segments deleted. First, Δ98Δ retains all the critical residues of the hydrophobic core, that is, those implicated in the nucleation event leading to the folded state. Second, the analysis of the putative structure through the identification and counting of amino acid neighbors and surface calculations predicts that removal of stretches 1−28 and 127−131 would have a relatively minor impact on the overall structure of IFABP. In particular, distance profiles show that those fragments are positioned furthest away from the hydrophobic core, whereas neighborhood maps reveal an imperfect hydrogen-bonding network between strand A and adjacent strands B and J. Moreover, minimal increases in nonpolar and total accessible surface area are expected from the excision of the fragments giving rise to the truncated form.

Naturally occurring β-sheet proteins avoid edge-to-edge aggregation through a variety of strategies (*29*). It is noteworthy that Δ98Δ lacks any tendency to aggregate under the conditions assayed. This happens despite the likely occurrence of free edges in the construct. In this regard, Δ98Δ might constitute a useful model to explore critical determinants leading to β-aggregates, a hot topic of study nowadays for its relevance in the formation of amyloid fibrils involved in a variety of diseases.

The results presented herein support a view by which Δ98Δ would adopt a conformation with a compact core and a loose periphery, representing so far the smallest structure of its kind preserving binding activity.

ACKNOWLEDGMENT

We are grateful to Dr. Cecilia Arighi for her observations which inspired the early stages of this work. We thank Ms. Gabriela Gómez for her critical reading of the final version of this manuscript. We are indebted to Dr. Oleg Tsodikov for generously providing the source code of his program Surface Racer and to Mr. Mario Cazeneuve for expediently adapting the software to comply with our needs.

REFERENCES

1. Banaszak, L., Winter, N., Xu, Z., Bernlohr, D. A., Cowan, S., and Jones, A. (1994) Lipid-binding proteins: a family of fatty acids and retinoid transport proteins, *Adv. Protein Chem. 45*, 89−151.
2. Ropson, I. J., Gordon J. I., and Frieden, C. (1990) Folding of a predominantly β-structure protein: intestinal fatty acid binding protein, *Biochemistry 29*, 9591−9599.

3. Hodson, M. E., and Cistola, D. P. (1997) Discrete backbone disorder in the nuclear magnetic resonance structure of apo-intestinal fatty acid-binding protein: implications for the mechanism of ligand entry, *Biochemistry 36*, 1450−1460.
4. Steel, R. A., Emmert D. A., Kao, J., Hodson, M. E., Frieden, C., and Cistola, D. P. (1998) The three-dimensional structure of a helix-less variant of intestinal fatty acid-binding protein, *Protein Sci. 7*, 1332−1339.
5. Ogbay, B., Dekoster, G. T., and Cistola, D. P. (2003) The NMR structure of a stable compact all-β-sheet variant of intestinal fatty acid-binding protein, *Protein Sci. 13*, 1227−1237.
6. Clérico, E. M., Peisajovich, S. G., Ceolín, M., Ghiringhelli, P. D., and Ermácora, M. R. (1999) Engineering of a compact non-native state of intestinal fatty acid binding protein, *Biochim. Biophys. Acta 1476*, 203−218.
7. Arighi, C. N., Rossi, J. P. F. C., and Delfino, J. M. (1998) Temperature-induced conformational transition of intestinal fatty acid binding protein enhancing ligand binding: a functional, spectroscopic, and molecular modeling study, *Biochemistry 37*, 16802−16814.
8. Arighi, C. N., Rossi, J. P. F. C., and Delfino, J. M. (2003) Temperature-induced conformational switch in intestinal fatty acid binding protein (IFABP) revealing an alternative mode for ligand binding, *Biochemistry 42*, 7539−7551.
9. Cull, M., and McHenry, C. S. (1990) Preparation of extracts from prokaryotes, *Methods Enzymol. 182*, 147−153.
10. Schägger, H., and von Jagow, G. (1987) Tricine-sodium dodecyl sulfate−polyacrylamide gel electrophoresis for the separations of proteins in the range from 1 to 100 kDa, *Anal. Biochem. 166*, 368−379.
11. Nozaki, Y. (1990) Determination of tryptophan, tyrosine and phenylalanine by second derivative spectrophometry, *Arch. Biochem. Biophys. 277*, 324−333.
12. Lakowicz, J. (1999) *Principles of Fluorescence Spectroscopy*, 2nd ed., p 54, Kluwer Academic/Plenum Publishers, New York, Boston, Dordrecht, London, and Moscow.
13. Weber, G. (1992) *Protein Interactions*, pp 177−198, Chapman & Hall Inc., New York.
14. Schmid, F. (1989) Spectral methods of characterizing protein conformation and conformational changes, in *Protein Structure: A Practical Approach* (Creighton, T. E., Ed.) p. 251, IRL, Oxford, New York, and Tokyo.
15. Uversky, V. N. (1993) Use of fast protein size-exclusion liquid chromatography to study the unfolding of proteins which denature through the molten globule, *Biochemistry 32*, 13288−13298.
16. Santoro, M. M., and Bolem, D. W. (1998) Unfolding free energy changes determined by the linear extrapolation method. 1. Unfolding of α-chymotrypsin using different denaturants, *Biochemistry 27*, 8063−8068.
17. Tsodikov O. V., Record, M. T., Jr., and Sergeev, Y. V. (2002) A novel computer program for fast and exact calculation of accessible and molecular surface areas and average surface curvature, *J. Comput. Chem. 23*, 600−609.
18. Yeh, S., Ropson, I. J., and Rousseau, D. L. (2001) Hierarchical folding of intestinal fatty acid-binding protein, *Biochemistry 40*, 4205−4210.
19. Butler, W. L. (1979) Fourth derivative spectra, *Methods Enzymol. 56*, 501−515.
20. Clérico, E. M., and Ermácora, M. R. (2001) Tryptophan mutants of intestinal fatty acid-binding protein: ultraviolet absorption and circular dichroism studies, *Arch. Biochem. Biophys. 395*, 215−224.
21. Creigthon, T. E. (1993) *Proteins: Structural and Molecular Properties*, 2nd ed., p 191, W. H. Freeman and Company, New York.
22. Clark, P. L., Liu, Z. P., Zhang, J., and Gierasch, L. M. (1996) Intrinsic tryptophan mutants as probes of structure and folding, *Protein Sci. 5*, 1108−1117.
23. Arai, M., and Kuwajima, K. (2000) Role of the molten globule state in protein folding, *Adv. Protein Chem. 53*, 209−282.
24. Cistola, D. P., Kim, K., Rogl, H., and Frieden, C. (1996) Fatty acid interactions with a helix-less variant of intestinal fatty acid-binding protein, *Biochemistry 35*, 7559−7565.
25. Flanagan, J. M., Kataoka, M., Shortle, D., and Engelman, D. M. (1992) Truncated staphylococcal nuclease is compact but disordered, *Proc. Natl. Acad. Sci. U.S.A. 89*, 748−752.
26. Fontana, A., Polverino de Laureto, P., Spolaore, B., Frare, E., Picotti, P., and Zambonin, M. (2004) Probing protein structure by limited proteolysis, *Acta Biochim. Pol. 51*, 299−321.
27. Kim, K., Cistola, D. P., and Frieden, C. (1996) Intestinal fatty acid-binding protein: the structure and stability of a helix-less variant, *Biochemistry 35*, 7553−7558.
28. Sacchettini, J. C., Gordon, J. I., and Banaszak, L. J. (1989) Crystal structure of rat intestinal fatty-acid-binding protein. Refinement and analysis of the *Escherichia coli*-derived protein bound with palmitate, *J. Mol. Biol. 208*, 327−339.
29. Richardson, J. S., and Richardson, D. C. (2002) Natural β-sheet proteins use negative design to avoid edge-to-edge aggregation, *Proc. Natl. Acad. Sci. U.S.A. 99*, 2754−2759.

BI051080S